Data-Driven Approach on the Mechanism of Radiative Collapse in the Large Helical Device*)

Tatsuya YOKOYAMA[1,2], Hiroshi YAMADA[1], Suguru MASUZAKI[3,4,5], Junichi MIYAZAWA[3,5], Kiyofumi MUKAI[3,5], Byron J. PETERSON[3,5], Naoki TAMURA[3,5], Ryuichi SAKAMOTO[3,5], Gen MOTOJIMA[3,5], Katsumi IDA[3], Motoshi GOTO[3,5], Tetsutaro OISHI[3,5], Gakushi KAWAMURA[3,5], Masahiro KOBAYASHI[3,5] and LHD Experiment Group[3]

[1]*Graduate School of Frontier Sciences, The University of Tokyo, Chiba 277-8561, Japan*
[2]*Research Fellow of Japan Society for the Promotion of Science, Tokyo 102-0083, Japan*
[3]*National Institute for Fusion Science, National Institutes of Natural Sciences, Gifu 509-5292, Japan*
[4]*Research Institute for Applied Mechanics, Kyushu University, Fukuoka 816-8580, Japan*
[5]*The Graduate University for Advanced Studies, SOKENDAI, Gifu 509-5292, Japan*

(Received 10 November 2020 / Accepted 17 December 2020)

A radiative collapse predictor has been developed using a machine-learning model based on high-density plasma experiments in the Large Helical Device (LHD). Concurrently, the physical background of radiative collapse was discussed based on the distinct features extracted by a sparse modeling, which is one of the frameworks of data-driven science. Electron density, CIV and OV line emissions, and electron temperature at the plasma edge have been extracted as the key parameters of radiative collapse. Those parameters are relevant to the physical knowledge that the major cause of radiative collapse is the enhancement of radiative loss by light impurities in the plasma-edge region. Using these four parameters, the likelihood of occurrence of radiative collapse has been estimated. The behavior of plasma at the edge—in particular, the carbon impurities outside the last closed flux surface—has been evaluated using EMC3-EIRENE code for the phase with increasing likelihood, that is, the plasma is getting close to the collapse. It is shown that the radiation caused by the C^{3+} ion, which corresponds to the CIV emission, is enhanced in the region where electron temperature is around 10 eV.

Keywords: Large Helical Device (LHD), radiative collapse, density limit, impurity, stellarator-heliotron plasma, sparse modeling, data-driven science, EMC3-EIRENE

DOI: 10.1585/pfr.16.2402010

1. Introduction

The most distinguished plasma termination event is disruption in the tokamaks. Even in stellarator-heliotron plasmas, which are free from disruption, radiative collapse is a major cause of plasma termination in a high-density regime and consequently limits operational density. The best-known empirical density limit for the stellarator-heliotron plasma is given by the Sudo density [1].

$$n_{\mathrm{e}}^{\mathrm{Sudo}}[10^{20}\mathrm{m}^{-3}] = 0.25P^{0.5}B^{0.5}a^{-1}R^{-0.5}. \quad (1)$$

Here, P is the absorbed power (MW), B is the magnetic field strength on the plasma axis (T), a is the average minor radius (m), and R is the major radius (m). In a theoretical study, the radiation caused by light impurities is regarded important in occurrence of radiative collapse [2]. The contributions of other operational conditions and plasma parameters, such as wall condition and impurity concentration, to the occurrence of radiative collapse could be important, but these contributions are hidden behind the expression of the Sudo scaling. In an early research on the density limit in the Large Helical Device (LHD), electron density was indicated to be greater than the Sudo limit by 40% [3].

In recent years, the data-driven approach using machine-learning techniques has gained attention in the study of disruption, which is a critical phenomenon in a tokamak. Disruption prediction studies based on machine-learning techniques were performed for many tokamaks [4–7]. In parallel with improvement of predictive capability, some studies suggested that it is important to reveal the physical implication of the predictor to develop a reliable predictor [8, 9].

In the present research, a model to predict the occurrence of radiative collapse has been constructed using a linear support vector machine (SVM) [10], which is one of the traditional machine-learning techniques. Data from density ramp-up experiments in LHD has been used to construct a dataset to train the model, and the plasma parameters which are relevant to radiative collapse have been extracted by the exhaustive search (ES), which is one of the sparse modeling techniques [11]. Based on the ex-

author's e-mail: yokoyama.tatsuya17@ae.k.u-tokyo.ac.jp
*) This article is based on the presentation at the 29th International Toki Conference on Plasma and Fusion Research (ITC29).

tracted parameters, the likelihood of the radiative collapse has been evaluated as an index between zero and one. Finally, the change in plasma was discussed during increases in likelihood, which indicates that the plasma gets close to collapse. EMC3-EIRENE code [12–14] was used to evaluate the plasma condition and the impurity radiation at the plasma edge. This code solves a steady-state distribution of the plasma and impurity using fluid equations along magnetic field lines and with cross-field diffusion.

This article is organized as follows. In section 2, the dataset and machine-learning model are described. Section 3 presents the result of ES and likelihood estimation based on the ES result. Impurity behavior in the edge region when the plasma approaches the collapse is discussed in section 4. Finally, section 5 concludes the article.

2. Construction of Classifier Model

2.1 Dataset

High-density hydrogen and deuterium plasmas in the LHD have been used to construct the dataset. In those experiments, the magnetic axis position R_{ax} was fixed at 3.6 m and the magnetic field at the magnetic axis in vacuum was either 1.375 T or 2.75 T. Neutral beam injection (NBI) was mainly used to heat plasma. The 15 plasma parameters listed in Table 1 have been considered in sparse modeling. The typical waveform of a discharge with radiative collapse is shown in Fig. 1.

Table 1 Plasma parameters used in the dataset.

Expression	Description
$\bar{n}_e$	Line averaged electron density [10^{19}m^{-3}]
B	Magnetic field at magnetic axis in vacuum [T]
P_{rad}/P_{abs}	Radiation loss normalized by absorbed input power
P_{abs}	Absorbed input power [MW]
β_{dia}	Diamagnetic beta value
Δ_{sh}	Shafranov shift [m]
a_{99}	Minor radius defined by the radius encompassing 99% of the stored energy [m]
CIII	CIII ($2s^2\ ^1S - 2s2p\ ^1P$, 97.7 nm) line intensity normalized by $\bar{n}_e$
CIV	CIV ($2s\ ^2S - 2p\ ^2P$, 154.9 nm) line intensity normalized by $\bar{n}_e$
OV	OV ($2s^2\ ^1S - 2s2p\ ^1P$, 63.0 nm) line intensity normalized by $\bar{n}_e$
OVI	OVI ($2s\ ^2S - 2p\ ^2P$, 103.4 nm) line intensity normalized by $\bar{n}_e$
FeXVI	FeXVI ($3s\ ^2S - 3p\ ^2P$, 33.5 nm) line intensity normalized by $\bar{n}_e$
$I_{sat}^{(7L)}$	Ion saturation current on a divertor target plate [A]
D/(H + D)	Ratio of deuterium ion to the sum of hydrogen ion and deuterium ions
$T_{e,edge}$	Electron temperature at the last closed flux surface (LCFS) in vacuum [keV]

In construction of the dataset, 71 discharges with collapses and 27 discharges without collapses were considered. The data in discharges with collapses were labeled as "close-to-collapse" and "stable" according to the normalized time derivatives of radiation power $x_{rad} = \dot{P}_{rad}/P_{rad}$. Here, the dots indicate time derivatives. This index is similar to the density exponent $x_{density} = (\dot{P}_{rad}/P_{rad})/(\dot{\bar{n}}_e/\bar{n}_e)$ [15] since the temporal change of density is slower than that of radiation power. The density exponent is a criterion that shows a relationship between radiation power and plasma density, and it is known that $x_{density}$ becomes ≥ 3 when a thermal instability occurs in the plasma. As seen in Fig. 1 (a), x_{rad} increases drastically as the plasma approaches radiative collapse. In such discharges, the phase with $x_{rad} > 2.5$ (hatched in red) was labeled as "close-to-collapse". In contrast, the plasma is regarded as "stable" against radiative collapse before x_{rad} reaches 2. Therefore, data of the phase with the same time width of the "close-to-collapse" phase before x_{rad} reaches 2 (hatched in blue) were labeled "stable". In the case of discharges without radiative collapse, the data between 4 s and 5 s have been labeled as "stable".

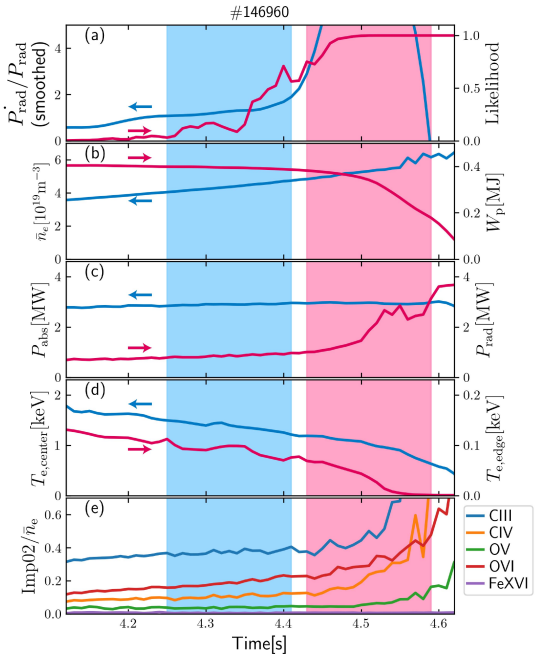

Fig. 1 Typical discharge with a radiative collapse in the dataset. The red and blue regions are "close-to-collapse" region and "stable" regions, respectively. (a) The normalized time derivatives of radiation power is shown in blue and collapse likelihood (described in sec 3) is shown in red. (b) Line-averaged electron density $\bar{n}_e$ is shown in blue, and diamagnetic stored energy W_p, in red. (c) Absorbed heating power P_{abs} is shown in blue,4 and radiation loss P_{rad}, in red. (d) Electron temperature at the plasma center $T_{e,center}$ is shown in blue, and that at plasma edge $T_{e,edge}$, in red. (e) Visible impurity line intensities normalized by $\bar{n}_e$ are shown.

2.2 Machine-learning model

To construct a predictor model, a linear SVM has been used as a basic two-class classifier. An SVM returns an equation of boundary between both classes, described as $f(\boldsymbol{x}) = 0$, where $\boldsymbol{x}$ is a vector of input parameters. The function $f(\boldsymbol{x})$ is called decision function and it is a linear function in a linear SVM as follows.

$$f(\boldsymbol{x}) = \boldsymbol{w}^T \boldsymbol{x} + b. \tag{2}$$

Here, the coefficients $\boldsymbol{w} \in \mathbb{R}^d$ and $b \in \mathbb{R}$ are called weight and bias, respectively. In the present study, the dataset is taken logarithms and min-max normalized before training the model. By this preprocessing, the decision function $f(\boldsymbol{x})$ is deformed into the exponential form $f_{\exp}(\boldsymbol{x})$. Note that the boundary equation is deformed as $f_{\exp}(\boldsymbol{x}) = 1$. In training the SVM, a concept called "soft-margin", which allows some data to inhabit the opposite side of the boundary, was used.

3. Collapse Likelihood Estimation

3.1 Feature extraction by exhaustive search

ES is one of sparse modeling techniques in the framework of data-driven science [11, 16]. Sparse modeling exploits the inherent sparseness in all high-dimensional data and enables us to extract information from data effectively. When selecting input parameters in a classification problem, it is necessary to consider not only the individual distribution of each parameter, but also the effect of combinations of parameters. In the ES, all possible combinations of parameters are evaluated and compared each other. To avoid overfitting to the training data, 10-fold cross validation was performed to evaluate each combination by generalization performance. F1-score [17], which is one of the metrics commonly used to evaluate machine learning classifiers, was used to evaluate the performance of the predictor.

From the ES results, a combination of four parameters have been selected as the key parameters, $\bar{n}_e$, CIV, OV, and $T_{e,edge}$. These parameters are included in many of the top combinations of the ES when limited to combinations of five parameters, as shown in Fig. 2. The decision function using these four key parameters, which defines the boundary in the multi-dimensional space, was obtained as follows.

$$f_{\exp}(\boldsymbol{x}) = \exp(-5.89)\bar{n}_e^{0.864}\mathrm{CIV}^{0.995}\mathrm{OV}^{-0.395}T_{e,edge}^{-1.85}. \tag{3}$$

3.2 Collapse likelihood

The collapse likelihood has been estimated by corresponding the distance from the boundary to the fitting of the frequency of the occurrence by the sigmoid function as follows.

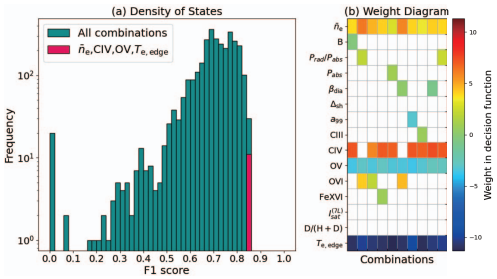

Fig. 2 Exhaustive search (ES) result when limited to combinations of 5 parameters. The blue and red bars in the left diagram show the distributions of F1-score with five parameters and that with the combinations including $\bar{n}_e$, CIV, OV, and $T_{e,edge}$. The right diagram shows the parameters included in the top-10 combinations in the F1-score. Each column corresponds to each combination, and the color bar corresponds to the weight in the decision function.

$$\text{Likelihood} = \frac{1}{1 + \exp\{-8.34\,(\log_{10} f(\boldsymbol{x}) + 0.3082)\}}. \tag{4}$$

The likelihood takes a continuous value from zero to one.

In the top panel of Fig. 1, the temporal change of collapse likelihood is shown by a red line. The likelihood is close to 0 while the plasma is stable, but increases to about 1 when the plasma approaches collapse.

4. Numerical Estimate of Carbon Radiation Distribution

According to Eq. 3, light impurities, especially carbon, seem to be important; this result agrees with previous theoretical research [2]. However, most of the $T_{e,edge}$ values used in the dataset are distributed around 100 eV, while the radiation rate of carbon has the first peak at around 10 eV [18]. Therefore it is necessary to investigate the region outside the LCFS to elucidate the physical mechanism of radiative collapse.

In the present research, the EMC3-EIRENE code has been used to evaluate the behavior of plasma with focus on carbon impurity outside the LCFS. Figure 3 shows the discharge with radiative collapse which was selected as a reference for the simulation. EMC3-EIRENE simulations were conducted for three time points shown by dotted lines in Fig. 3. In these simulations, the diffusion coefficient of carbon D_C and the carbon sputtering yield were fixed so that the distribution of C^{6+} ion becomes close to that was measured by charge exchange spectroscopy [19] at 4.31 s.

The distributions of radiation power caused by the C^{3+} ion, which corresponds to the CIV line emission, against T_e at each location are shown in Fig. 4 for each time point. According to Fig. 4, C^{3+} radiation was enhanced when the electron temperature was less than 47.9 eV, which is the third ionization potential of carbon. As the plasma approached the collapse and the likelihood increased, whole radiation power resulting from C^{3+} increased. More-

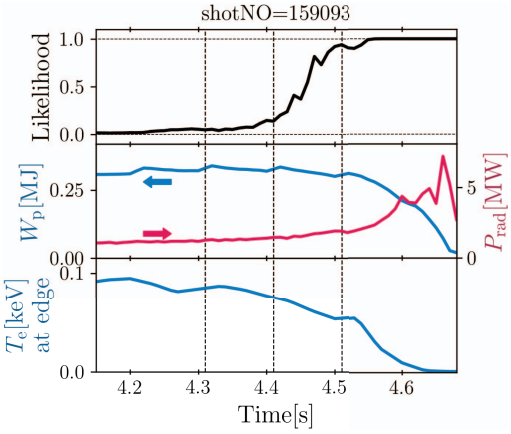

Fig. 3 Reference discharge with radiative collapse for EMC3-EIRENE simulation. The top panel shows the temporal change of collapse likelihood. In the bottom panel, diamagnetic energy W_p and P_{rad} are shown by blue and red lines, respectively.

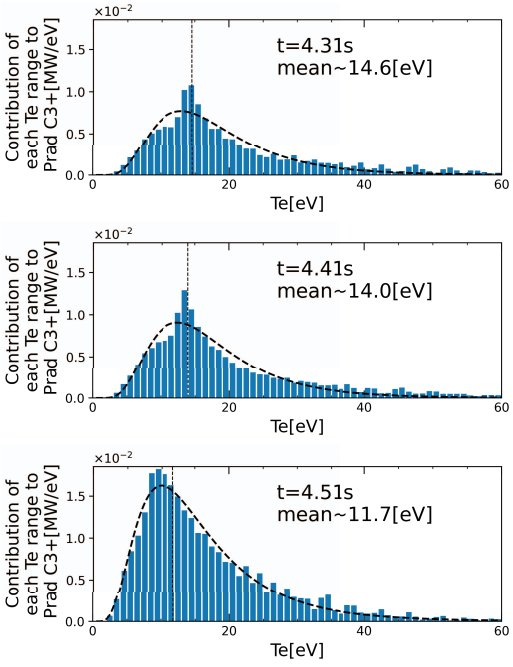

Fig. 4 Contribution of each range of electron temperature T_e for radiation power caused by C^{3+} ion. From the top to the bottom, the results at 4.31 s, 4.41 s, and 4.51 s are shown. The dashed curves show the curves fitted by a logarithmic normal distribution, and the vertical dashed lines show the mean temperature of the fitted curves.

over, the mean temperatures, which were located between 10 and 15 eV, slightly shifted toward lower temperatures when approaching collapse. Consequently, the change in radiation power caused by C^{3+} was observed before the collapse occurs. The increase of radiation was remarkable in the region with an electron temperature of around 10 eV. This change in radiation is supposed to be caused by decrease of electron temperature and increase in C^{3+} density, and future work will tackle the task of identification of the factors leading to increase in radiation.

5. Conclusion

In the present study, a radiative collapse predictor model has been developed using the SVM based on high-density experiment data in LHD. The features of radiative collapse have been extracted by the ES, which is one of a sparse modeling technique. From the ES results, the combination of $\bar{n}_e$, CIV, OV, and $T_{e,edge}$ has been selected as the key factor for radiative collapse. These parameters were used to estimate the likelihood of radiative collapse. This predictor model based on the likelihood will be applied to control LHD plasma in the near future to avoid radiative collapse.

To reveal the mechanism of radiative collapse, this study has focused on the plasma-edge region and the time range in which the collapse likelihood increases. For three time points in this range, EMC3-EIRENE simulations were performed to evaluate the behavior of carbon impurities. The radiation from C^{3+} ion was found to be concentrated where the electron temperature is around 10 eV. Further investigation based on the simulation result and measured data is underway.

Acknowledgements

This work is supported by the National Institute for Fusion Science grant administrative budgets NIFS18KLPP051, and JSPS KAKENHI Grant Numbers JP19J20641 and JP19H05498.

[1] S. Sudo *et al.*, Nucl. Fusion **30**(1), 11 (1990).
[2] K. Itoh, S.-I. Itoh and L. Giannone, J. Phys. Soc. Jpn. **70**(11), 3274 (2001).
[3] B.J. Peterson *et al.*, Phys. Plasmas **8**(9), 3861 (2001).
[4] A. Murari *et al.*, Nucl. Fusion **59**(8), 086037 (2019).
[5] C. Rea *et al.*, Nucl. Fusion **59**(9), 096016 (2019).
[6] A. Pau *et al.*, IEEE Trans. Plasma Sci. **46**(7), 2691 (2018).
[7] J. Kates-Harbeck, A. Svyatkovskiy and W. Tang, Nature **568**(7753), 526 (2019).
[8] T. Yokoyama *et al.*, Fusion Eng. Des. **140**, 67 (2019).
[9] C. Rea *et al.*, Fusion Sci. Technol. **76**(8), 912 (2020).
[10] C. Cortes and V. Vapnik, Machine Learning **20**(3), 273 (1995).
[11] Y. Igarashi *et al.*, J. Phys. Conf. Series **699**(1), 012001 (2016).
[12] Y. Feng *et al.*, Contrib. Plasma Phys. **44**(1-3), 57 (2004).
[13] D. Reiter, M. Baelmans and P. Börner, Fusion Sci. Technol. **47**(2), 172 (2005).
[14] G. Kawamura *et al.*, Plasma Phys. Control. Fusion **60**(8), 084005 (2018).
[15] B.J. Peterson *et al.*, Plasma Fusion Res. **1**, 045 (2006).
[16] Y. Igarashi *et al.*, J. Phys. Conf. Series **1036**, 012001 (2018).
[17] C. Van Rijsbergen, *Information Retrieval* (Butterworths, London, 1979).
[18] D. Post *et al.*, Atomic Data Nucl. Data Tables **20**(5), 397 (1977).
[19] K. Ida and S. Hidekuma, Rev. Sci. Instrum. **60**(5), 867 (1989).